Scattering from nonlinear gravity waves: the "choppy wave" model

Frédéric Nouguier, Charles-Antoine Guérin and Bertrand Chapron*

May 5, 2010

Abstract

To progress in the understanding of the impact of non-linear wave profiles in scattering from sea surfaces, a non-linear model for infinite depth gravity waves is considered. This model, termed the "Choppy Wave Model" (CWM), is based on horizontal deformation of a linear, reference random surface. It is numerically efficient and enjoys explicit second-order statistics for height and slope, which makes it well adapted to a large family of scattering models. We incorporate the CWM into a Kirchhoff or Small-Slope Approximation and derive statistical expressions for the corresponding incoherent cross section. We insist on the importance of "undressing" the wavenumber spectrum to generate a non-linear surface with a prescribed spectrum. Interestingly, the inclusion of non-linearities is found to be practically compensated by the spectral undressing process, an effect which might be specific to the CWM and needs to be investigated in the framework of fully non-linear models. Accordingly, the difference between the respective NRCS is rather small. The most noticeable changes are faster azimuthal variations and a slight increase of the radar returns at nadir. A statistical analysis of sea clutter in the framework of a Two-Scale Model is also performed at large but nongrazing incidence. It shows a pronounced polarization dependence of the distribution of large backscattered amplitudes, the tail being much larger in horizontal polarization and for small resolution cell. Surface non-linearities are shown to increase the tail of the amplitude distribution, as expected. Less obviously, their relative impact is found lesser in horizontal polarization. This raises the question of the actual contribution of non-linearities in radar sea spikes at nongrazing angles.

1 Introduction

The modeling of electromagnetic wave scattering from sea surfaces has been a constantly evolving field of research since more than half a century [1], trig-

*F. Nouguier and B. Chapron are with the IFREMER, Laboratoire d'Océanographie Spatiale, 29280 Plouzané, France, C-A. Guérin is with the LSEET, UMR CNRS 6017, and Université du Sud-Toulon-Var, Avenue de l'Université, BP 20132 F-83957 La Garde cedex

gered by a large number of ocean remote sensing applications. For near-nadir geometry in the upper bands of the microwave regime, radar back-scattering measurements exhibit very little polarization dependency but some evidences of frequency sensitivity. Accordingly, the Physical Optics or Kirchhoff approximation (henceforth referred to as KA) has been invoked to interpret radar back scatter measurement. At larger but still moderate angles, more elaborate models must be invoked to account for the polarization dependence, but many of them are based on local curvature corrections to the KA, which is essentially a tangent plane approximation (e.g. [2, 3]).

As the scattering models gain in reliability, it becomes all the more crucial to consider an accurate statistical description of the sea surface. One key issue is to better take into account the non-linearity of surface waves and the resulting non-Gaussian heights and slopes distributions. The non-Gaussian features of the surface distribution have two important consequences. First, they affect the value of the incoherent NRCS which are usually calculated within a Gaussian framework. Second, they modify the modeling and interpretation of sea clutter. The purpose of this paper is to address both issues in a unified framework.

The aforementioned KA scattering solution, as well as other more elaborate scattering models, directly depends upon the two-points characteristic function of elevations. In the case of a Gaussian distribution, the characteristic function can simply be expressed in terms of the correlation function. To incorporate non-Gaussian effects in scattering calculations, third or fourth order cumulant functions, which involve the so-called skewness and peakedness functions, must be considered. These functions are generally unknown and have only been treated in the limit of Geometrical Optics (GO), by fitting their asymptotic form around zero with slope distribution ([4]). *Ad hoc*, rather arbitrary, analytical expressions have then been assumed for these functions away from zero ([2, 5, 6, 7]). Other attempts have been made to incorporate the geometrical effect of steep (but non-breaking) waves in approximate scattering models through a modification of the shadowing function [8] or the facet slope distribution in the Two-Scale Model [9]. Another approach is purely numerical and consists in a Monte-Carlo average of the NRCS over a large number of non-linear samples sea surfaces ([10, 11, 12, 13, 14]). This technique, however, remains essentially limited to one-dimensional surfaces or small sea patches.

In the last few years, there has been a renewal of interest in Lagrangian description of sea surface, after the pioneering work of Pierson [15, 16]. This representation has proved to be advantageous in several respects. It allows fast and accurate numerical generation of fully two-dimensional sample sea surfaces, together with the analytical derivation of some statistical properties of the sea surface. In this framework, the authors recently analyzed a simple non-linear model [17] for infinite depth gravity waves, referred to as the Choppy Wave Model (CWM), whose main properties are recalled in section II. It is based on first-order expansions of particle trajectories in Lagrangian coordinates. At first order in surface curvature, this representation is found equivalent to other existing weakly non-linear solutions. Moreover, CWM is numerically efficient and enjoys explicit second-order statistics. It is thus particularly well adapted

to the calculation of NRCS with analytical methods involving the two-point characteristic function (section III and IV). A similar Lagrangian model was already considered in the framework of a KA approximation [18]. However, a crucial aspect was seemingly omitted. Indeed, it is essential to consider a preliminary step, which we refer to as the "undressing procedure" of the initial spectrum (section V). This enables one to generate non-linear waves with a prescribed spectrum and to provide "fair" comparisons between the NRCS from linear and non-linear waves (section VI). As we will show, changing a linear to a non-linear model induces only small modification of the magnitude of the incoherent NRCS. This is due to the undressing effect which partly cancels the effect of more peaky waves. Yet, a modified azimuthal behavior is obtained, with an increased directivity. In addition to the analytical tractability of the CWM for the incoherent NRCS, the numerical efficiency of the model allows one to simulate a two-dimensional sea clutter for realistic sea surfaces (section VII). As we will show, the clutter statistics of the CWM exhibit some differences with respect to the case of linear surfaces. In particular, the occurrence of burst or "sea spikes" is enhanced at large incidence angles, a phenomenon which is mirrored by a slower decay of the distribution of field amplitudes. This phenomenon is more pronounced for small resolution cell, where the deviation from the classical Rayleigh distribution for the field amplitude is very marked, especially in horizontal polarization. However, the relative contribution of surface non-linearities to the tail of the distribution is found smaller in horizontal than vertical polarization, a result which is far from being obvious.

2 The choppy waves model

The terminology of the CWM originates from the choppy aspect of the waves generated by this technique. The model is not properly new, as it has been used for years by the computer graphics community.

The CWM is based on a Lagrangian approach and takes into account the horizontal displacement of particles. Thus it can logically be expressed as an horizontal deformation of a reference linear surface, instead of vertical one as most weakly non-linear models do. Assuming a representation of the linear sea surface as a function $z = h(\mathbf{r}, t)$, where $\mathbf{r} = (x, y)$ is the horizontal coordinate, the CWM is obtained by the following transformation:

$$(\mathbf{r}, h(\mathbf{r}, t)) \mapsto (\tilde{\mathbf{r}}, \tilde{h}(\tilde{\mathbf{r}}, t)) \tag{1}$$

where the new coordinates are defined by:

$$\tilde{\mathbf{r}} = \mathbf{r} + \mathbf{D}(\mathbf{r}, t) \tag{2}$$

$$\tilde{h}(\tilde{\mathbf{r}}, t) = h(\mathbf{r}, t) \tag{3}$$

The displacement $\mathbf{D}$ is the so-called Riesz Transform of the function h:

$$\mathbf{D}(\mathbf{r}, t) = \int \mathbf{dk}\ \mathrm{i}\frac{\mathbf{k}}{k} \mathrm{e}^{\mathrm{i}\mathbf{k}\cdot\mathbf{r}} \hat{h}(\mathbf{k}, t) \tag{4}$$

where

$$\widehat{h}(\mathbf{k},t) = \frac{1}{(2\pi)^2}\int_{\mathbb{R}^2} \mathbf{dr}\ \mathrm{e}^{-\mathrm{i}\mathbf{k}\cdot\mathbf{r}} h(\mathbf{r},t) \tag{5}$$

is the two-dimensional spatial Fourier transform. The transformation (1) implicitly defines a modified process $\tilde{h}(\tilde{\mathbf{r}},t)$, which has been shown to possess non-Gaussian height and slope distributions, as well as a modified spectrum. A complete statistical description of the resulting process has been established in [17], whenever the reference surface is a stationary centered Gaussian process and will be partly used in the following.

3 Scattering under the Kirchhoff/Small-Slope Approximation

3.1 The scattering amplitude

Consider an incident linearly polarized monochromatic plane wave $\mathbf{E}_i(\mathbf{R}) = \mathrm{e}^{\mathrm{i}\mathbf{K}_0\cdot\mathbf{R}}\mathbf{E}_0$ impinging on the sea surface at incidence angle θ_0 and giving rise to a scattered field $\mathbf{E}_s$ above the surface. The geometry of the problem is depicted on Figure 1.

As usual, a $\mathrm{e}^{-i\omega t}$ time dependence is implicitly assumed. Following the standard notation, we decompose the wave vectors into horizontal and vertical components,

$$\mathbf{K}_0 = \mathbf{k_0} - q_0\widehat{\mathbf{z}},\ \mathbf{K} = \mathbf{k} + q\widehat{\mathbf{z}}, \tag{6}$$

with $q, q_0 > 0$ and $k_0^2 + q_0^2 = k^2 + q^2 = K_0^2 = (2\pi/\lambda)^2$. It is also convenient to introduce the Ewald vector $\mathbf{Q} = \mathbf{K} - \mathbf{K}_0$ and its components $\mathbf{Q_H} = \mathbf{k} - \mathbf{k_0}$, $Q_z = q + q_0$. The scattering amplitude in the KA approximation is written:

$$\mathbb{S}(\mathbf{K},\mathbf{K}_0) = \frac{\mathbb{N}(\mathbf{K},\mathbf{K}_0)}{Q_z}\frac{1}{(2\pi)^2}\int_{\mathbb{R}^2} \mathbf{d\tilde{r}}\ \mathrm{e}^{\mathrm{i}\mathbf{Q_H}\cdot\tilde{\mathbf{r}}}\mathrm{e}^{\mathrm{i}Q_z\tilde{h}(\tilde{\mathbf{r}})}, \tag{7}$$

where $\mathbb{N}(\mathbf{K},\mathbf{K}_0)$ is a kernel depending on the frequency, the polarization, the scattering angles and the complex permittivity of the lower medium. The expression of the kernel can be found for example in the Appendix E of [1].

To calculate the scattered amplitude (7), the idea is to perform a change of variables $\tilde{\mathbf{r}} = \mathbf{r} + \mathbf{D}(\mathbf{r})$, assuming this change of variables to be univocal (no loop). This turns the integrand into explicit quantities:

$$\mathbb{S}(\mathbf{K},\mathbf{K}_0) = \mathbb{N}(\mathbf{K},\mathbf{K}_0)\ \frac{1}{(2\pi)^2}\int_{\mathbb{R}^2} \mathbf{dr}\ \mathrm{e}^{\mathrm{i}\mathbf{Q_H}\cdot\mathbf{r}}\mathrm{e}^{\mathrm{i}Q_z h(\mathbf{r})+\mathrm{i}\mathbf{Q_H}\cdot\mathbf{D}(\mathbf{r})}J(\mathbf{r}), \tag{8}$$

where the Jacobian of the transformation is given by:

$$J(\mathbf{r}) = \begin{vmatrix} 1+\partial_x D_x(\mathbf{r}) & \partial_x D_y(\mathbf{r}) \\ \partial_y D_x(\mathbf{r}) & 1+\partial_y D_y(\mathbf{r}) \end{vmatrix}$$

The numerical evaluation of the KA scattering amplitude for a sample sea surface requires the generation of the processes $h(\mathbf{r}), \mathbf{D}(\mathbf{r})$ and $J(\mathbf{r})$. These

quantities can be generated efficiently by Fast Fourier Transform (FFT). While a linear surface only necessitates one two-dimensional FFT (2D-FFT), the CWM requires 5 additional 2D-FFT: 2 for the displacement vector $\mathbf{D}$ and 3 for the Jacobian components (note that $\partial_x D_y = \partial_y D_x$). Altogether, the generation of a non-linear sample surface for scattering purpose is only 6 times as long as in the linear case. The validity of the formula (8) is conditioned by the univocity of the change of variables, that is $J(\mathbf{r}) > 0$. This is not a drastic condition as the derivatives of D have the same magnitude as the corresponding slope process and are therefore a few times smaller than one.

The expression (8) of the scattering amplitude can also be used for another common asymptotic theory, namely the first-order Small-Slope Approximation (SSA1) of Voronovich [19]. We recall that KA and SSA1 only differ by the geometrical kernel $\mathbb{N}(\mathbf{K}, \mathbf{K}_0)$, which depends solely on the scattering angles and the complex permittivity. In the following , we will refer to KA-CWM or SSA1-CWM to designate the KA or SSA1 NRCS in the framework of the CWM.

3.2 Derivation of the incoherent NRCS

The reference linear surface is modeled by a Gaussian stationary process, with given spectrum (Γ) and correlation function (C). The incoherent NRCS is the limit of the statistical average

$$\sigma^{(0)} = \frac{4\pi}{|A|}\left(\left\langle |\mathbb{S}|^2 - |\langle \mathbb{S} \rangle|^2 \right\rangle\right) \tag{9}$$

for an infinite illuminated area $|A|$. In the framework of the KA/SSA1 approximation it is given by

$$\sigma^{(0)} = 4\pi \left|\frac{\mathbb{N}}{Q_z}\right|^2 \Psi \tag{10}$$

with

$$\Psi = \frac{1}{(2\pi)^4}\frac{1}{|A|}\int_{A\times A} \mathbf{d\tilde{r}}\, \mathbf{d\tilde{r}'}\, \mathrm{e}^{\mathrm{i}\mathbf{Q_H}\cdot(\tilde{\mathbf{r}}-\tilde{\mathbf{r}}')}\left(\left\langle \mathrm{e}^{\mathrm{i}Q_z(\tilde{h}(\tilde{\mathbf{r}})-\tilde{h}(\tilde{\mathbf{r}}'))}\right\rangle - \left\langle \mathrm{e}^{\mathrm{i}Q_z\tilde{h}(\tilde{\mathbf{r}})}\right\rangle\left\langle \mathrm{e}^{-\mathrm{i}Q_z\tilde{h}(\tilde{\mathbf{r}}')}\right\rangle\right) \tag{11}$$

Performing the double change of variable $\tilde{\mathbf{r}} = \mathbf{r} + \mathbf{D}(\mathbf{r})$ and $\tilde{\mathbf{r}}' = \mathbf{r}' + \mathbf{D}(\mathbf{r}')$ lead to

$$\begin{aligned}\Psi \;=\; & \frac{1}{(2\pi)^4}\frac{1}{|A|}\int_{A\times A} \mathbf{dr}\, \mathbf{dr}'\, \mathrm{e}^{\mathrm{i}\mathbf{Q_H}\cdot(\mathbf{r}-\mathbf{r}')}\left(\left\langle J(\mathbf{r})J(\mathbf{r}')\mathrm{e}^{\mathrm{i}Q_z(h(\mathbf{r})-h(\mathbf{r}'))+\mathrm{i}\mathbf{Q_H}.(\mathbf{D}(\mathbf{r})-\mathbf{D}(\mathbf{r}'))}\right\rangle\right. \\ & \left. - \left\langle J(\mathbf{r})\mathrm{e}^{\mathrm{i}Q_z h(\mathbf{r})+i\mathbf{Q_H}.\mathbf{D}(\mathbf{r})}\right\rangle\left\langle J(\mathbf{r}')\mathrm{e}^{-\mathrm{i}Q_z h(\mathbf{r}')-i\mathbf{Q_H}.\mathbf{D}(\mathbf{r}')}\right\rangle\right)\end{aligned} \tag{12}$$

Since the underlying Gaussian process is stationary, the quantity under brackets depend only the difference $\mathbf{r} - \mathbf{r}'$ and the double integral can be reduced to a single one:

$$\Psi = \int_{\mathbb{R}^2} \mathbf{dr}\left[\left\langle \mathrm{e}^{\mathrm{i}Q_z(h(\mathbf{r})-h(\mathbf{0}))+i\mathbf{Q_H}.(\mathbf{D}(\mathbf{r})-\mathbf{D}(\mathbf{0}))}J(\mathbf{r})J(\mathbf{0})\right\rangle - \left|\left\langle \mathrm{e}^{\mathrm{i}Q_z h(\mathbf{r})+i\mathbf{Q_H}.\mathbf{D}(\mathbf{r})}J(\mathbf{r})\right\rangle\right|^2\right]\mathrm{e}^{\mathrm{i}\mathbf{Q_H}.\mathbf{r}} \tag{13}$$

Discarding the quadratic terms in D_x, D_y (which are of the order of the mean square slope) we may approximate:

$$J(\mathbf{r}) = 1 + \nabla \cdot \mathbf{D}(\mathbf{r}) + \partial_x D_x(\mathbf{r})\partial_y D_y(\mathbf{r}) - \partial_x D_y(\mathbf{r})\partial_y D_x(\mathbf{r}) \simeq 1 + \nabla \cdot \mathbf{D}(\mathbf{r}) \quad (14)$$

leading after tedious but straightforward calculations (using the statistical expressions recalled in the Appendix) to the following expression of the functional $\tilde{\Psi}$:

$$\Psi = \int_{\mathbb{R}^2} \mathbf{dr}\ \mathrm{e}^{\mathrm{i}\mathbf{Q_H}\cdot\mathbf{r}} \left[\exp\left(-\frac{Q_z^2}{2} S_0 \right) \mathcal{F}(\mathbf{r}) - \mathrm{e}^{-Q_z^2\sigma_0^2} \mathcal{F}(\infty) \right] \quad (15)$$

where

$$\mathcal{F} = \exp\left(-\frac{Q_H^2}{2} S_{\widehat{\mathbf{Q}}_H} \right) \left([1 - \mathrm{i}\mathbf{Q_H}.\nabla C]^2 - \Delta C + \frac{Q_z^2}{4} S_1^2 \right) \quad (16)$$

The functions S_0, S_1 and $S_{\widehat{\mathbf{Q}}_H}$ are auxiliary functions recalled in the Appendix. They are related to the spectrum Γ of the reference linear surface.

4 Spectral undressing

Following a terminology introduced by [20] we will qualify by "dressed" a spectrum which is actually measured experimentally, including non-linearities ($\tilde{h}$). The "bare" or "undressed" spectrum pertains to the linear surface that underlies the non-linear process (h). The dressed spectrum has a richer high-frequency content that the undressed one. One of the major difficulties in using non-linear models based on transformation of a reference process is to control the dressed spectrum at high frequencies. For this, it is necessary to rely on a transformation from undressed to dressed quantities, an equation which we will call a "dressing formula". In the following we will write with a tilde superscript any function referring to a dressed quantity. Whenever the reference linear surface is a stationary Gaussian process, the transformed surface after the CWM is again stationary but non-Gaussian, with power spectrum $\tilde{\Gamma}$:

$$\tilde{\Gamma}(\mathbf{k}) = \frac{1}{(2\pi)^2} \int_{\mathbb{R}^2} \mathbf{dr}\ \mathrm{e}^{\mathrm{i}\mathbf{k}\cdot\mathbf{r}} \left(\gamma(\mathbf{r};\mathbf{k}) - \gamma(\infty;\mathbf{k}) \right), \quad (17)$$

where

$$\gamma(\mathbf{r};\mathbf{k}) = \left[\frac{-S_0}{2} \left((1 - \mathrm{i}\mathbf{k}\cdot\nabla C)^2 - \Delta C \right) + \frac{S_1^2}{4} \right] \mathrm{e}^{-\frac{k^2}{2} S_{\mathbf{k}}} \quad (18)$$

Again, the functions S_0, S_1 and $S_{\mathbf{k}}$ are auxiliary functions recalled in the Appendix. They are related to the undressed spectrum Γ of the reference linear surface. Note that γ is not a true correlation function, but only a convenient auxiliary function. As it depends on the $\mathbf{k}$ variable itself it is not the Fourier transform of the spectrum $\tilde{\Gamma}$. We note in passing that the actual dressed correlation function does not enjoy a simple analytical expression. The undressing procedure, i.e. the extraction of the original spectrum Γ from this relation, can

be realized efficiently by an iterative procedure (see section 3.3 of [17] for the details). In the case of anisotropic spectra, it is important to note that both the omnidirectional curvature and spreading functions must undergo simultaneously the undressing procedure. We will here limit the study to spectra with a second harmonic:

$$\tilde{\Gamma}(\mathbf{k}) = \frac{\tilde{B}(k)}{2\pi k^4}(1 + \tilde{\Delta}(k)\cos(2\varphi_{\mathbf{k}})), \tag{19}$$

where $\tilde{B}(k)$ is the omnidirectional curvature, $\tilde{\Delta}(k)$ the spreading function and $\varphi_{\mathbf{k}}$ the azimuthal angle with respect to the wind direction. Assuming a similar form for the undressed spectrum with some other quantities $\Gamma(\mathbf{k})$, $B(k)$ and $\Delta(k)$, one can define the curvature transfer function (CTF) and the spreading transfer function (STF) by:

$$CTF(k) = \frac{B(k)}{\tilde{B}(k)},\ STF(k) = \frac{\Delta(k)}{\tilde{\Delta}(k)} \tag{20}$$

Figures 2 and 3 show the curvature and spreading transfer function for a directional Elfouhaily spectrum [21]. As can be seen, the effect of undressing is very pronounced for the spreading function at high wave numbers, but remains within a few percent correction for the omnidirectional curvature. This relatively small effect might be due to the specific properties of the CWM and should not be understood as evidence that the spectral undressing procedure need not be considered. Today, the question of undressing effect according to a fully non-linear model is an open problem.

4.1 Scattering diagrams

The incoherent NRCS in the KA-CWM approximation has been implemented after formula (15) for a directional Elfouhaily spectrum. An accurate evaluation of this expression is non-trivial and requires the use of polar coordinates and special functions (see the Appendix). For a fair comparison with the linear case, the spectrum has been preliminarily undressed. In the following we will denote simply by KA the Kirchhoff NRCS calculated for a linear surface with a prescribed spectrum and KA-CWM the Kirchhoff NRCS for a non-linear surface with a dressed spectrum identical to the prescribed spectrum.

The most notable change of the KA-CWM with respect to KA is a tilt of the angular dependence of the exponential $\exp(-Q^2 S_0)$, where the factor Q_z is replaced by Q. The main consequence is to accelerate the damping effect of the exponential as one leaves the specular direction. This is, however, partly compensated for by the undressing of the spectrum, which makes the input structure function S_0 actually smaller than the one used under the linear assumption. Altogether, this appears to be a subtle compensation effects. Figures 4 and 5 display the upwind unpolarized monostatic NRCS as a function of the incidence and azimuth angle for the KA and KA-CWM. The diagrams in the incidence plane show little difference between the two models for a wind speed

of 7 m.s^{-1}, with a maximum variation of the order of 1 dB. Note, however, that the small difference (about half dB) observed may result in important bias when it comes to the estimation of the mean square slope from a Geometrical Optics fit. Moreover, even if the azimuthal variation amplitude of the NRCS is reduced in the KA-CWM, the azimuthal diagram (figure 5) shows a stronger sensibility of the NRCS to the wind direction, in the sense that the angular variation rate is increased. These observations are consistent with the aforementioned property of undressing, which affects essentially the directionality of the spectrum but not its magnitude, even for light winds.

For multiscale surfaces such as the sea surface in the microwave regime, it is well known that the Physical Optics approximation is an incomplete theory, as it is unable to account for the diffraction by small ripples and the polarization dependence. While the Physical Optics is sufficiently accurate at small angles, the need for a unified theory is crucial at higher scattering angles. Traditionally, one resorts to a Two-Scale Model (TSM) to incorporate the effects of both large scale tilting and small-scale Bragg scattering. In the TSM, the surface is represented by a superposition of a large- and small-scale processes, respectively whose power spectra are the restriction of the surface spectrum to its low- and high-frequency content, respectively. In the traditional TSM, the incoherent NRCS writes as a superposition of the Geometrical Optics (GO) cross-section of large scales and a Bragg cross-section in the local reference plane of the tilted rough facets, average over the distribution of facet slopes. The separation scale is usually set around the Bragg frequency Q_H. The arbitrariness of this cut-off has been for a long time an issue of the TSM. Recently, it was shown that an improved TSM based on a combination of the GO and a tilted SSA1 (rather than GO and a tilted Bragg) is quasi insensitive to the cut-off. The model was termed GO-SSA [22].

The adaptation of a TSM to non-linear surfaces is problematic in view of the hydrodynamic modulation of small- by large-scales which does not allow to separate the scales. For this reason we did not succeed in deriving a statistical formula for the NRCS in the GO-SSA model for CWM. However, tilting effects can be re-introduced in the framework of Monte-Carlo averaging over rough facets, as will be done in the next section for the clutter analysis.

5 Sea clutter under the Two-Scale Model

Even through the CWM might be less accurate than existing higher-order non-linear theories, a big asset of the model is its numerical efficiency. This makes it possible to generate realistic sea surfaces with ordinary numerical facilities. One can thus describe the non-linear wave interactions over the full range of scales, including the peak waves and the short gravity waves. We have used this possibility to simulate the sea clutter in L band as it can for instance be observed on a RAR image or in the temporal fluctuation of the cross-section measured over a single small patch of sea as was done in [23]. The reason for choosing the L band (1.3 GHz) is the possibility to consider sample surface larger than a few

peak wavelengths and thus the ability to take into account the hydrodynamic modulation of small waves by larger waves. Sample surfaces of 220 m $\times$ 220 m by a wind speed of 11 m/s have been generated with a sampling rate of 3 cm, which sets the shortest wave to 6 cm. For this, the numerical generation technique described in [17] has been applied to a directional Elfouhaily spectrum with preliminary undressing. Every pixel of the image can be simulated by associating a back-scattering cross-section to every small patch of the surface. This can be realized by means of a tapered, moving incident beam. Specifically, we have used the technique developed in [24] to calculate the cross-section of deterministic rough surface illuminated by Gaussian beams, in the framework of Kirchhoff-like scattering models. The KA-CWM or SSA1-CWM scattering amplitude for a finite illumination is given by

$$\mathbb{S}(\mathbf{K},\mathbf{K}_0) = \mathbb{N}(\mathbf{K},\mathbf{K}_0)\ \frac{1}{(2\pi)^2}\int_{\mathbb{R}^2} \mathbf{dr}\ \mathrm{e}^{\mathrm{i}\mathbf{Q_H}\cdot\mathbf{r}}\mathrm{e}^{\mathrm{i}Q_z h(\mathbf{r})+\mathrm{i}\mathbf{Q_H}\cdot\mathbf{D}}J(\mathbf{r})g(\mathbf{r})d\mathbf{r}, \qquad (21)$$

where g is a Gaussian window which limits the area of illumination. This expression was shown to be accurate at non-grazing incidence as soon as the footprint is a few times larger than the incident wavelength. The Gaussian window has been regularly translated and re-centered over every cell of the surface, to simulate the contribution of every elementary patch of the surface. The footprints of the translated beams overlap in such a way that the total illumination on the surface is quasi-uniform. We have gradually set the standard deviation of g to 0.62, 1.25 and 2.5 m, so that every single beam practically isolates resolution cells of 2.5, 5 and 10 m diameter, respectively. We have not investigated the grazing regime, which necessitates very large footprints and is numerically too demanding.

For simplicity, the cell is assumed to be square, even though range resolved cells are usually much wider in the azimuthal direction. We do not, however, claim to simulate a realistic SAR image which is distorted by several artifacts linked to the Doppler processing (essentially velocity bunching) and cannot be modeled in such a simple manner. Our simulation is more relevant in the context of a RAR image or to model the time series than can be obtained from the echo of a unique resolution cell (assuming that the temporal fluctuations of a single cell are statistically identical to the spatial variations of many different cells in a larger footprint).

For large angles, it is well known that the radar return exhibits a strong polarization dependence, making KA irrelevant. On the other hand, SSA1 does not comply to the tilt-invariance property of the scattering amplitude ([1]) and is not adapted to fully developed sea surfaces, which can have non-negligible local facet slopes, especially at large scattering angles. This results in an overestimation of the polarization ratio. To introduce a nontrivial polarization dependence, it is necessary to account for the facet tilting in the expression of the SSA1-CWM. This can easily be done by replacing the geometrical kernel in front of the Kirchhoff integral (21) by the Bragg kernel $\mathbb{B}$ associated to the

reference frame of the rough facet of normal $\widehat{\mathbf{n}}$:

$$\mathbb{N}(\mathbf{K}, \mathbf{K}_0) \rightarrow \mathbb{B}(\mathbf{K}, \mathbf{K}_0; \widehat{\mathbf{n}}) \tag{22}$$

The expression of the tilted Bragg tensor can be found e.g. in [22]. In the numerical simulations $\widehat{\mathbf{n}}$ is taken as the normal vector of the mean facet inside the pixel. As a consequence, the distribution of such normal vectors depends on the size of the resolution cell. The resulting scattering model will be termed TSSA1-CWM ("T" for "tilted").

Figures 6 displays the image that can be obtained by calculating the elementary back-scattering cross-section in the TSSA1-CWM model (including undressing and tilting kernel) at an incidence angle of 70 degrees for the HH polarization. The elementary cross-sections have been normalized by their mean value over the entire footprint. In the top panel, the color scale has been thresholded to 4.5 times the average value to obtain a better contrast. In the bottom panel, the color scale ranges from 4 to 6.5 times the average value to better evidence the bright spots, corresponding to occurrence of large echo usually referred to as "sea spikes". The modulation by the large scales is visible on the top panel through the alternating bright and dark regions. The occurrence of sea spikes is visible on the bottom panel, where only extreme values have been retained. As expected, the frequency of sea spikes is increased in the CWM with respect to the linear surface model. A similar but less pronounced behavior is obtained for the VV polarization.

To quantify the enhancement of sea spikes, it is instructive to look at the clutter statistics. This statistics is relevant to model the temporal statistics obtained by measuring with a fixed radar the varying cross section over a small sea patch (such as in the experiment of [23]) or the spatial statistics of a RAR image with the same pixel size. Following the standard methodology, we will consider the probability distribution function (p.d.f) of scattered amplitude rather than intensity. In this variable, the distribution is known to be Rayleigh under the assumption of a Gaussian field. Figure 7 and 8 show the p.d.f of the normalized amplitude $u = \sqrt{\sigma^{(0)}}/\langle\sqrt{\sigma^{(0)}}\rangle$ in semi-logarithmic axes for the different pixel sizes and polarizations at the same incidence of 70 degrees. The oscillations observed at the larger resolution cell is due to the limited occurrence of large amplitudes. Smoother distributions would require a large number of sample surfaces, which could not be achieved within a reasonable computational time.

The Rayleigh distribution $p(u) = u/\sigma \exp(-u^2/(2\sigma^2))$ is given for reference, with a parameter $\sigma = \sqrt{2/\pi}$ providing a mean value of 1. In the case of linear surfaces and vertical polarization (Figure 7), the p.d.f is increasingly well approached by a Rayleigh distribution as the pixel size is augmented. The TSSA1-CWM model, however, exhibits a distribution of amplitudes with larger tail, which favors the occurrence of large amplitudes, especially for small cell resolution. In horizontal polarization (Figure 8), the deviation from the Rayleigh distribution is found much larger for both the linear and CWM sea surface model. As expected, the amplitude distribution in the TSSA1-CWM has a slower decrease than in the corresponding linear case, but the relative difference

between the two distributions is found smaller than for the vertical polarization. This seems to indicate that the most important contribution to the heavy tail of the field amplitude is the tilt-variability of the HH Bragg-Kernel, which is much greater than the VV one. This behavior is consistent with the experimental clutter data presented in [23] in similar conditions (their figure 10), at least qualitatively. A more quantitative criterion is the probability of exceeding some given threshold, say three times the mean value, for the scattering amplitude. Numerical integration of the p.d.f for the finest resolution (2.5 m) yields an exceeding probability of 0.0016 (linear surfaces) and 0.0026 in vertical polarization versus 0.013 and 0.015 in horizontal polarization. This supports the counter-intuitive idea that the relative enhancement of the tail of the distribution is weaker in horizontal polarization. This raises the question of the true contribution of non-linearities in radar spikes at large but nongrazing angles.

Numerical simulations on weakly non-linear one-dimensional surfaces after the Creamer model have been performed recently with a rigorous scattering model [13] at large and grazing angles. The results obtained at various bands and resolutions also suggest a pronounced effect of polarization on the clutter distribution, with a much larger tail in horizontal polarization. Regarding the impact of non-linearities, it was also observed that the effect of "turning off" the non-linearities (their Figure 11) is stronger in vertical than horizontal polarization, as far as large amplitudes are concerned. We only compare qualitative results, as the cited test case addresses a different configuration (X band, 5 m/s wind speed at 85 incidence angle, one-dimensional Creamer surfaces with a rigorous EM solution). A definitive answer to the true origin of large amplitude in the horizontally polarized clutter will only be given by running a rigorous electromagnetic code on a fully non-linear 2D-surface model, a problem which seems for the moment to be a very difficult task.

Clutter statistics are often fitted with K- or Weibull distributions, which exhibit such heavy tails. The cumulative function F of the latter is of the form:

$$F(u) = 1 - \exp(-C\ u^{\alpha}) \tag{23}$$

To characterize the tail of the distribution, it is useful to use the so-called Weibull-paper, in which the above function transforms to a straight line of slope α:

$$v = \log_{10}(u) \tag{24}$$

$$w = \log_{10}\left(\ln \frac{1}{1-F(u)}\right) \tag{25}$$

Figure 9 shows the cumulative distribution in Weibull paper for the linear and CWM surface in HH polarization. In this representation, all distributions are found to be linear at small and intermediate values but grow sub-linearly at the very end of the distribution, which implies a tail decaying slower than Weibull distributions. This result is somewhat different from the findings of [13], where a good match was found with the latter law. This difference might be due either to an inaccuracy of our combined TSSA1-CWM model or to the specificity of the

regime in consideration (1D versus 2D results, X-band versus L-band, grazing versus moderate angles). The difference between the linear and CWM model is more pronounced for small amplitudes. Again, this seems to indicate that the main source of large amplitude in HH polarization is the tilting effect rather than the non-linear model. All these issues remain to be investigated.

6 Conclusion

The CWM is a non-linear surface model based on horizontal deformation of a reference linear surface. This defining property makes it adapted to the calculation of the scattered amplitude in the framework of analytical scattering theories such as the Kirchhoff and Small-Slope Approximation. A statistical formula for the incoherent NRCS has been derived, involving the spectrum and correlation function of the reference Gaussian surface. We have insisted on the importance of undressing the spectrum before any non-linear transformation is applied to the latter, to avoid the introduction of artificial high-frequency components in the non-linear surface. The main outcome of the numerical trials is that the introduction of the CWM in the KA/SSA1 framework at moderate incidence has a limited impact on the magnitude of the back-scattering cross-section, but a pronounced effect on the azimuthal behavior of the NRCS. The CWM combined with a Two-Scale Model has been applied to the simulation of two-dimensional sea clutter in L band at large incidence angles. The main observations can be summarized as follows:

- the tail of the back-scattered amplitude distribution is much larger in horizontal polarization and close to the reference Rayleigh distribution in vertical polarization.
- the deviation to the Rayleigh distribution strongly depends on the smallness of the resolution cell.
- the relative enhancement of the tail of the distribution due to the presence of surface non-linearities is stronger in vertical than horizontal polarization.

The present study is far from being complete. It is well known that the contribution of hydrodynamic non-linearities to the Doppler echo is very important, even through less visible on the NRCS. The investigation of Doppler signatures in the framework of the CWM is underway and is left for further study.

Appendix

6.1 Correlation and structure functions

In the following we denote $\widehat{\mathbf{u}} = \mathbf{u}/u$ the unitary vector which gives the direction of a vector u. The correlation function C is defined by:

$$C(\mathbf{r}) = \int \mathrm{e}^{\mathrm{i}\mathbf{k}\cdot\mathbf{r}}\Gamma(\mathbf{k})d\mathbf{k} \tag{26}$$

The structure function S_0 is defined by:

$$S_0(\mathbf{r}) = 2(C(0) - C(\mathbf{r})) \tag{27}$$

The Gilbert transform of the correlation and structure functions are defined by:

$$\begin{aligned} C_1(\mathbf{r}) &= \int \mathrm{e}^{\mathrm{i}\mathbf{k}\cdot\mathbf{r}} k\ \Gamma(\mathbf{k})d\mathbf{k} & (28)\\ S_1(\mathbf{r}) &= 2(C_1(0) - C_1(\mathbf{r})) & (29) \end{aligned}$$

The Riesz transform of the correlation function is defined by:

$$\mathbf{C}_{\mathcal{R}}(\mathbf{r}) = \int \mathrm{e}^{\mathrm{i}\mathbf{k}\cdot\mathbf{r}}(\mathrm{i}\widehat{\mathbf{k}})\ \Gamma(\mathbf{k})d\mathbf{k} \tag{30}$$

We also introduce

$$S_{\widehat{\mathbf{u}}}(\mathbf{r}) = 2\int_{\mathbb{R}^2} \mathbf{dk}'(\widehat{\mathbf{u}}\cdot\widehat{\mathbf{k}}')^2\Gamma(\mathbf{k}')[1 - \mathrm{e}^{\mathrm{i}\mathbf{k}'.\mathbf{r}}] \tag{31}$$

The following relations are consequences of standard properties of the characteristic functions of Gaussian processes:

$$\begin{aligned} \langle h(\mathbf{r})h(0)\rangle &= C(\mathbf{r}) & (32)\\ \langle [h(\mathbf{r}) - h(0)]^2\rangle &= S_0(\mathbf{r}) & (33)\\ \langle \exp(\mathrm{i}Q_z[h(\mathbf{r}) - h(0)]\rangle &= \exp(-Q_z^2/2\ S_0(\mathbf{r})) & (34)\\ \langle (\mathbf{Q_h}\cdot\mathbf{D})\exp(\mathrm{i}Q_z[h(\mathbf{r}) - h(0)]\rangle &= -\mathrm{i}Q_z C_{\mathcal{R}}(\mathbf{r})\exp(-Q_z^2/2\ S_0(\mathbf{r})) & (35)\\ \langle (\nabla\cdot\mathbf{D})\exp(\mathrm{i}Q_z[h(\mathbf{r}) - h(0)]\rangle &= -\mathrm{i}Q_z S_1(\mathbf{r})\exp(-Q_z^2/2\ S_0(\mathbf{r})) & (36) \end{aligned}$$

6.2 Spectra with two azimuthal harmonics

In the case of spectra with two azimuthal harmonics, the correlation functions and related Kirchhoff integrals can be efficiently computed with the help of Bessel functions. Consider a spectrum of the form:

$$\Gamma(\mathbf{k}) = \Gamma_0(k) + \Gamma_2(k)\cos(2\varphi_{\mathbf{k}}), \tag{37}$$

where $\varphi_{\mathbf{u}}$ indicates the azimuthal angle of a vector $\mathbf{u}$ with respect to the wind direction. Then the correlation function has also two harmonics:

$$C(\mathbf{r}) = [\Gamma_0]_0(r) - [\Gamma_2]_2(r)\cos(2\varphi_{\mathbf{r}}), \tag{38}$$

where $[f]_n$ denotes the Bessel transform of the radial function $f(k)$:

$$[f]_n(r) = 2\pi \int_0^\infty f(k) J_n(kr)\ k\ dk \tag{39}$$

Similarly we have (omitting the r variable for simplicity):

$$\begin{aligned} \Delta C &= -[k^2\Gamma_0]_0 + [k^2\Gamma_2]_2 \cos(2\varphi_{\mathbf{r}}) && (40)\\ C_1 &= [k\Gamma_0]_0 - [k\Gamma_2]_2 \cos(2\varphi_{\mathbf{r}}) && (41) \end{aligned}$$

With some algebra we obtain also:

$$\widehat{\mathbf{Q_H}}.\nabla C = -\cos(\varphi_{\mathbf{Q}_H}\varphi_{\mathbf{r}})[k\Gamma_0]_1 \tag{42}$$

$$\frac{1}{2}\left[(\{[k\Gamma_2]_1 - [k\Gamma_2]_3)\cos(\varphi_{\mathbf{r}} - \varphi_{\mathbf{Q}_H})\cos(2\varphi_{\mathbf{r}}) + (([k\Gamma_2]_1 + [k\Gamma_2]_3)\sin(\varphi_{\mathbf{r}} - \varphi_{\mathbf{Q}_H})\sin(2\varphi_{\mathbf{r}})\right]$$

$$S_{\widehat{\mathbf{Q_H}}} = \frac{1}{2}([\Gamma_0]_0 - [\Gamma_0]_2)\cos^2(\varphi_{\mathbf{Q}_H} - \varphi_{\mathbf{r}}) + \frac{1}{2}([\Gamma_0]_0 + [\Gamma_0]_2)\sin^2(\varphi_{\mathbf{Q}_H} - \varphi_{\mathbf{r}}) \tag{43}$$

$$\frac{1}{2}[\Gamma_2]_2\cos(2\varphi_{\mathbf{r}}) + \frac{1}{4}([\Gamma_2]_0 + [\Gamma_2]_4)\cos(2\varphi_{\mathbf{r}} - 2\varphi_{\mathbf{Q}_H})\cos(2\varphi_{\mathbf{r}}) + \frac{1}{4}([\Gamma_2]_0 - [\Gamma_2]_4)\sin(2\varphi_{\mathbf{r}} - 2\varphi_{\mathbf{Q}_H})\sin(2\varphi_{\mathbf{r}})$$

References

[1] T. Elfouhaily and C.A. Guérin. A critical survey of approximate scattering wave theories from random rough surfaces. *Waves in Random and Complex Media*, 14(4):1–40, 2004.

[2] AA Mouche, B. Chapron, N. Reul, D. Hauser, and Y. Quilfen. Importance of the sea surface curvature to interpret the normalized radar cross section (DOI 10.1029/2006JC004010). *J. Geophys. Res.*, 112(C10):10002, 2007.

[3] C.A. Guérin, G. Soriano, and B. Chapron. The weighted curvature approximation in scattering from sea surfaces. *Waves in Random and Complex Media*, 2010. submitted to Waves in Random and Complex Media.

[4] C. Cox and W. Munk. Statistics from the sea surface derived from the sun glitter. *J. Marine Res.*, 13:198–227, 1954.

[5] K.S. Chen, A.K. Fung, and D.E. Weissman. A backscattering model for ocean surfaces. *IEEE Trans. Geosci. and Remote Sens.*, 30(4):811–817, 1992.

[6] K.S. Chen, A.K. Fung, and F. Amar. An empirical bispectrum model for sea surface scattering. *IEEE Trans. Geosci. and Remote Sens.*, 31(4):830–835, 1993.

[7] C. Bourlier. Azimuthal harmonic coefficients of the microwave backscattering from a non-gaussian ocean surface with the first-order ssa model. *IEEE Trans. Geosci. and Remote Sens.*, 42(11):2600–2611, 2004.

[8] I.M. Fuks and A.G. Voronovich. Radar backscattering from Gerstner's sea surface wave. *Waves in Random and Complex Media*, 12(3):321–339, 2002.

[9] NI Nickolaev, OI Yordanov, and MA Michalev. Radar backscattering from non-Gaussian sea surface. In *Geoscience and Remote Sensing Symposium, 1991. IGARSS'91. Remote Sensing: Global Monitoring for Earth Management., International*, volume 3, 1991.

[10] J.T. Johnson, J.V. Toporkov, and G.S. Brown. A numerical study of backscattering from time-evolving sea surfaces: comparison of hydrodynamic models. *IEEE Trans. Geosci. and Remote Sens.*, 39(11):2411–2420, 2001.

[11] A.R. Hayslip, J.T. Johnson, and G.R. Baker. Further numerical studies of backscattering from time-evolving nonlinear sea surfaces. *IEEE Trans. Geosci. and Remote Sens.*, 41(10):2287–2293, 2003.

[12] G.Soriano, M.Joelson, and M.Saillard. Doppler spectra from a two-dimensional ocean surface at l-band. *IEEE Trans. Geosci. and Remote Sens.*, 44(9):2430–2437, 2006.

[13] JV Toporkov and MA Sletten. Statistical properties of low-grazing range-resolved sea surface backscatter generated through two-dimensional direct numerical simulations. *IEEE Transactions on Geoscience and Remote Sensing*, 45(5 Part 1):1181–1197, 2007.

[14] J.T. Johnson, R.J. Burkholder, J.V. Toporkov, D.R. Lyzenga, and W.J. Plant. A Numerical Study of the Retrieval of Sea Surface Height Profiles From Low Grazing Angle Radar Data. *IEEE Transactions on Geoscience and Remote Sensing*, 47:1641–1650, 2009.

[15] Jr W.J. Pierson. Perturbation analysis of the navier-stokes equations in lagrangian form with selected linear solutions. *Jour. Geophys. Res. B*, 67(8), 1962.

[16] Jr W.J. Pierson. Models of random seas based on the lagrangian equations of motion. Technical report, New York Univ., Coll. of Eng. Res. Div., Dept. of Meteorology and Oceanography, April 1961. Tech. Rep. prepared for the Office of Naval Research under contract Nonr-285(03).

[17] F. Nouguier, C.A. Guérin, and B. Chapron. 'Choppy wave' model for nonlinear gravity waves. *Journal of Geophysical Research (Oceans)*, 114(C13):09012, 2009.

[18] G. Engen, I. Friestad-Pedersen, H. Johnsen, and T. Elfouhaily. Curvature effects in ocean surface scattering. *IEEE Trans. Antennas Propag.*, 54(5):1370–1379, 2006.

[19] A. G. Voronovich. Small-Slope Approximation for electromagnetic wave scattering at a rough interface of two dielectric half-spaces. *Waves in Random Media*, 4:337–367, 1994.

[20] T. Elfouhaily, D. Thompson, D. Vandemark, and B. Chapron. Weakly nonlinear theory and sea state bias estimation. *J. Geophys. Res.*, 104(C4):7641–7647, 1999.

[21] T. Elfouhaily, B. Chapron, K. Katsaros, and D. Vandemark. A unified directional spectrum for long and short wind-driven waves. *J. Geophys. Res.*, 102(C7):15781–15796, July 1997.

[22] G. Soriano and C. Guérin. A cutoff invariant two-scale model in electromagnetic scattering from sea surfaces. *IEEE Geoscience and Remote Sensing Letters*, 5(2):199, 2008.

[23] DR Thompson and BL Gotwols. Comparisons of model predictions for radar backscatter amplitude probability density functions with measurements from SAXON. *Journal of Geophysical Research-Oceans*, 99(C5), 1994.

[24] G. Soriano, C.A. Guérin, and M. Saillard. Scattering by two-dimensional rough surfaces: comparison between the method of moments, Kirchhoff and small-slope approximations. *Waves in random media*, 12(1):63–84, 2002.

Acknowledgments

This work was supported by the ANR project no. ANR-09-BLAN-0232-01 SIMODE. F. Nouguier has been funded by the Direction Générale de l'Armement and IFREMER.

List of Figures

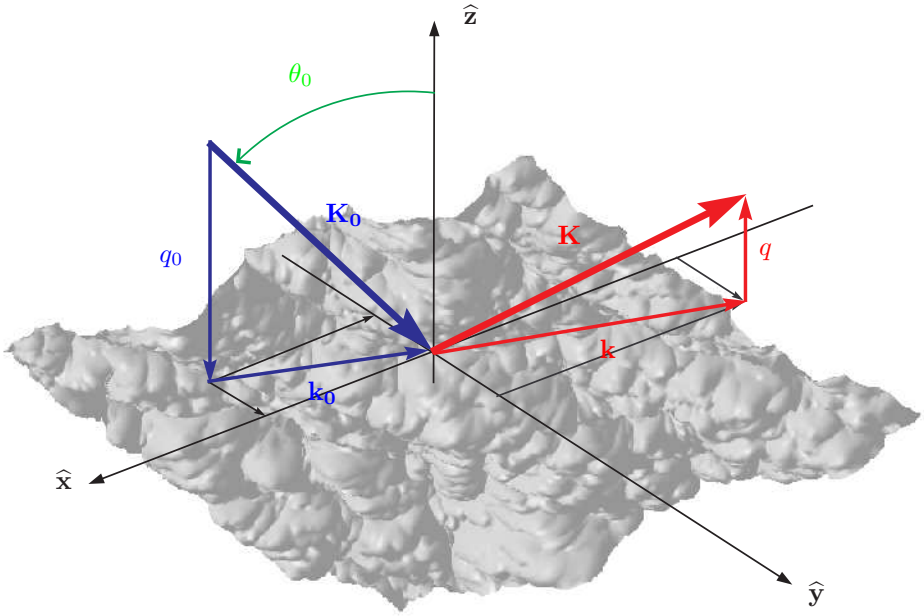

Figure 1: Geometry of the scattering problem

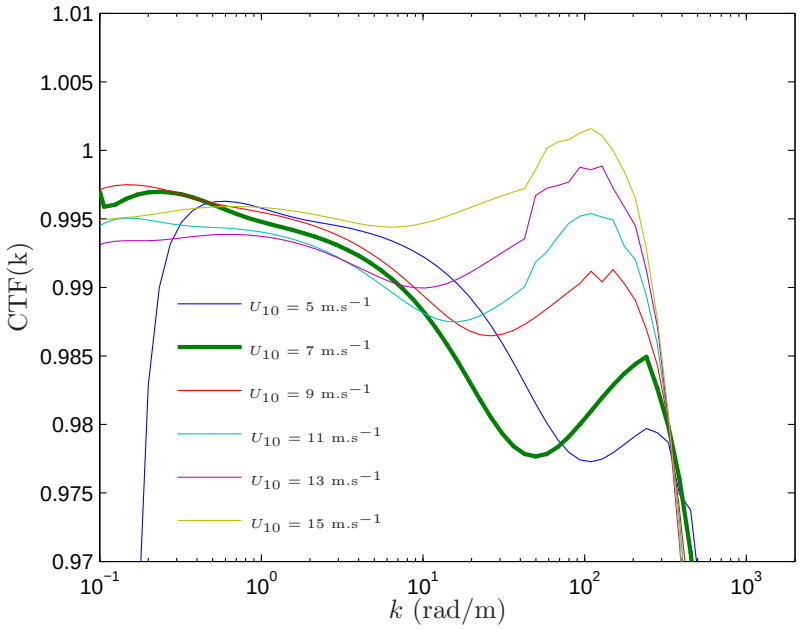

Figure 2: Curvature transfer function for the curvature at various wind speeds

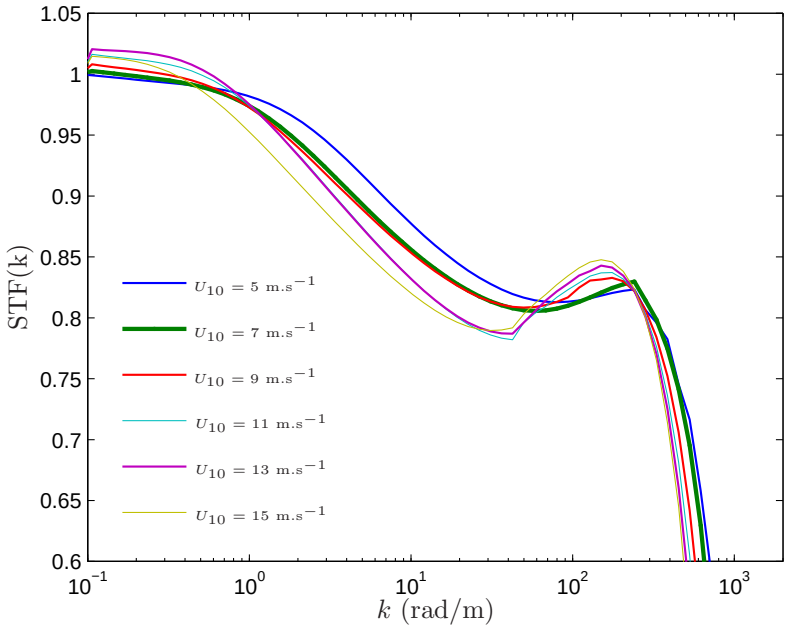

Figure 3: Spreading transfer function for the spreading at various wind speeds

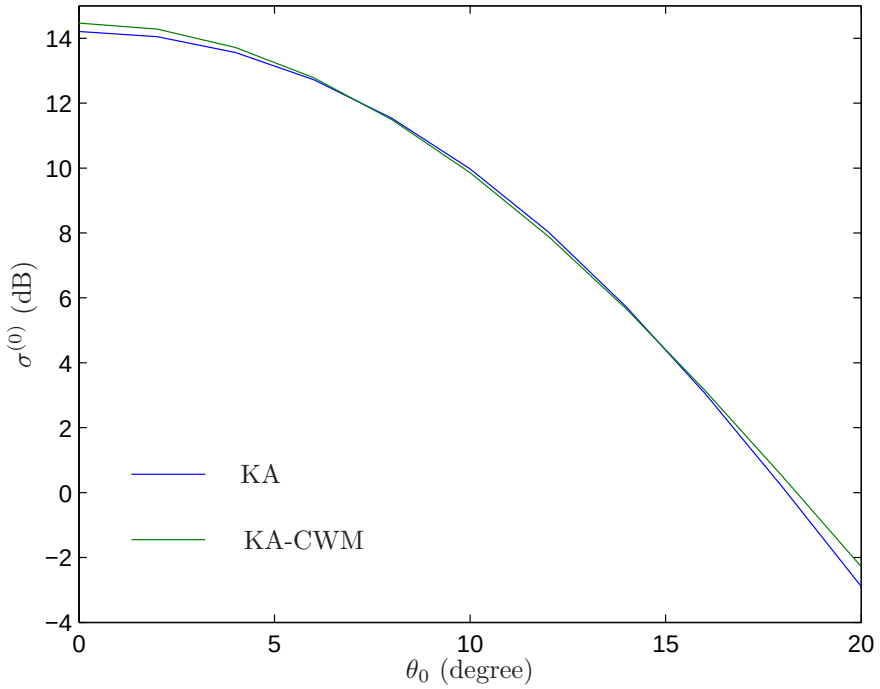

Figure 4: Upwind monostatic NRCS in C band under the KA and KA-CWM model, for a 7 m/s wind speed

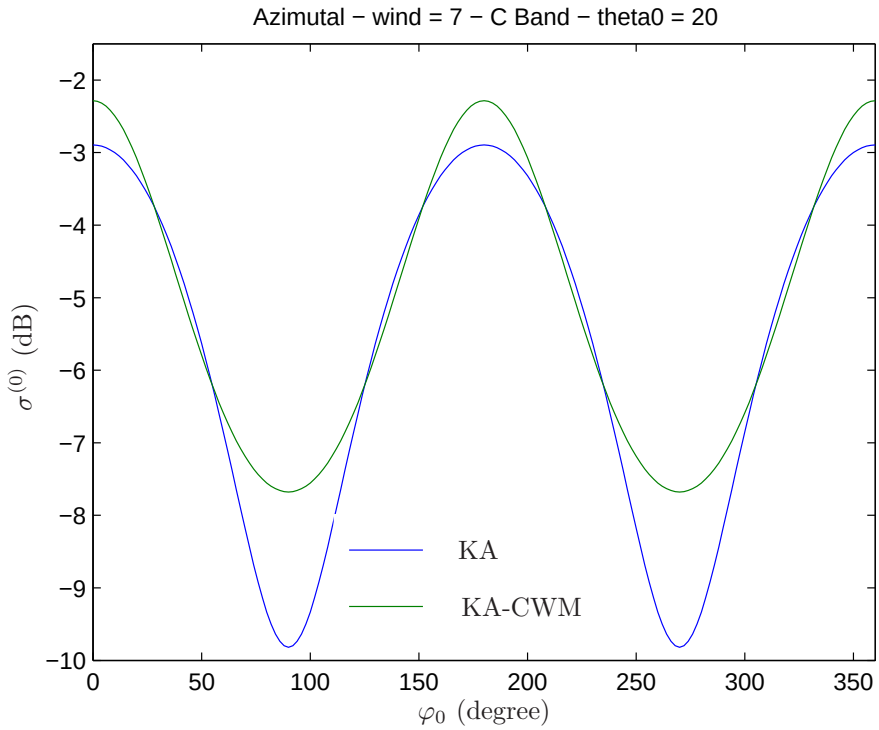

Figure 5: Azimuthal NRCS at 20 degrees in C band under the KA and KA-CWM model for a 7 m/s wind speed

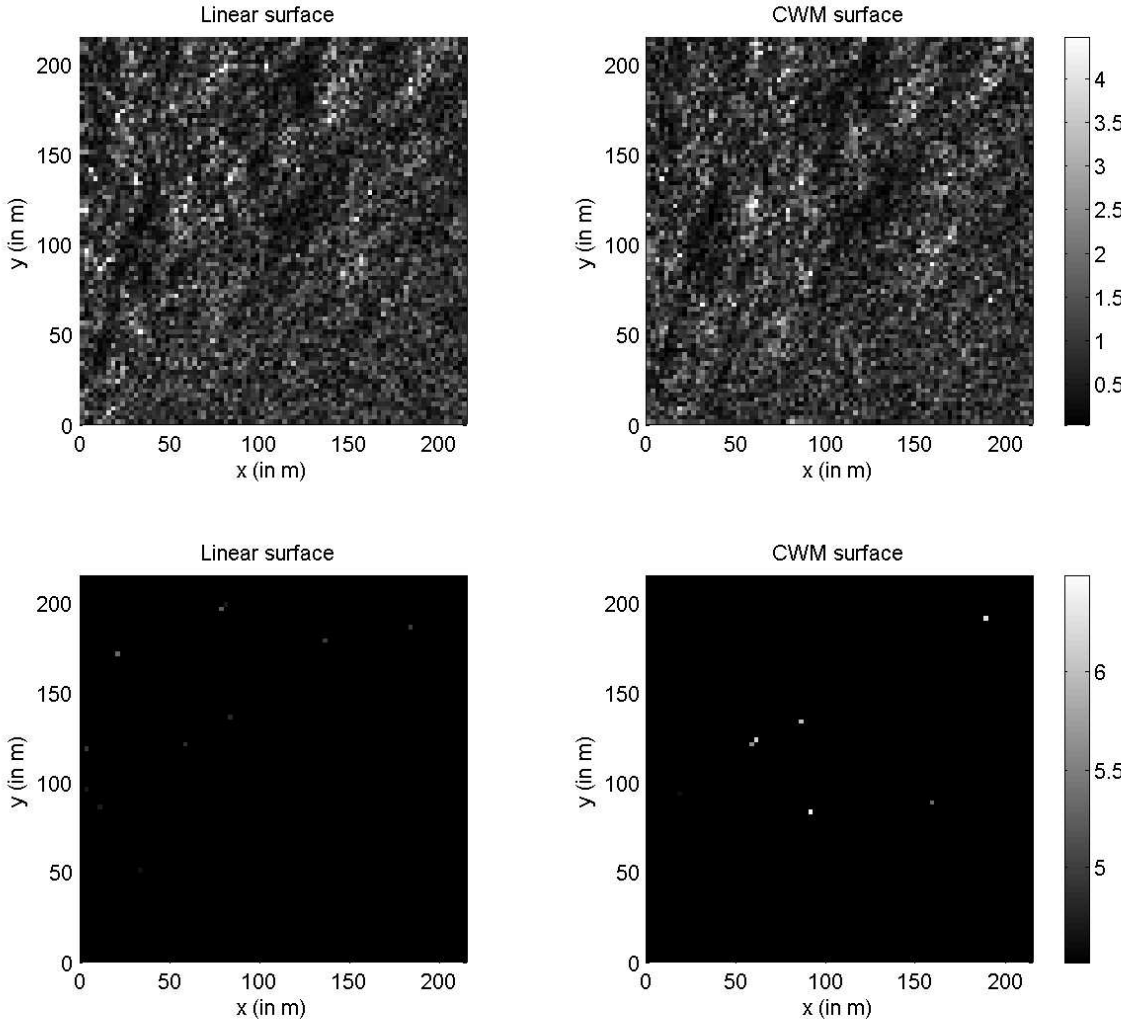

Figure 6: Image of sea clutter obtained in the tilted SSA1 (left) and TSSA1-CWM (right) models in HH polarisation. Each pixel represents a 2.5 m x 2.5 m patch on the surface. The incidence angle is 70 degrees. The top and bottom panel present the same image with different colorscales, to evidence the modulation by large waves (top panel) and the increased occurrence of sea-spikes in the CWM (bottom panel)

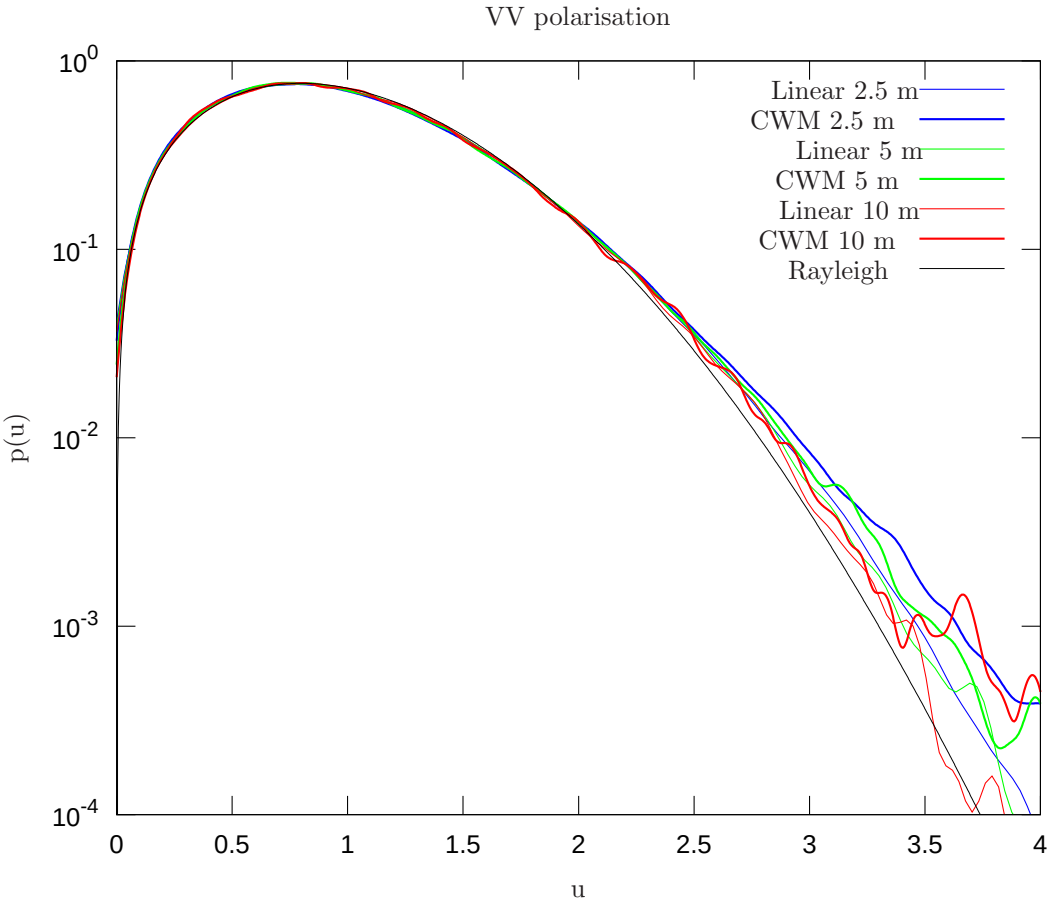

Figure 7: Probability density function of the back-scattering amplitude (normalized by its mean) in VV polarisation over the different resolution cells (upwind, L-band, 70 degrees incidence, wind speed 11 m/s). Here and in the following figures, the numbers in the legend (2.5 m, 5 m, 10 m) indicate the resolution cell.

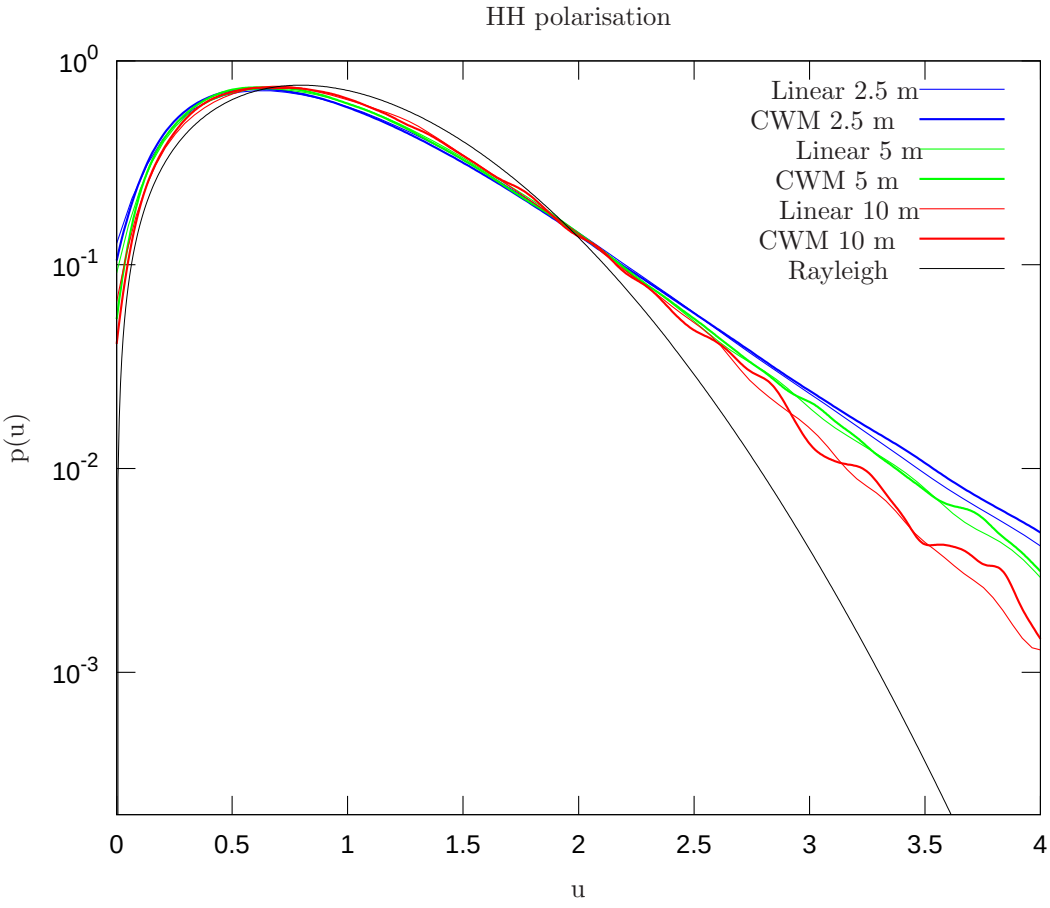

Figure 8: Probability density function of the backscattering amplitude (normalized by its mean) in HH polarisation over the different resolution cells (upwind, L-band, 70 degrees incidence, wind speed 11 m/s).

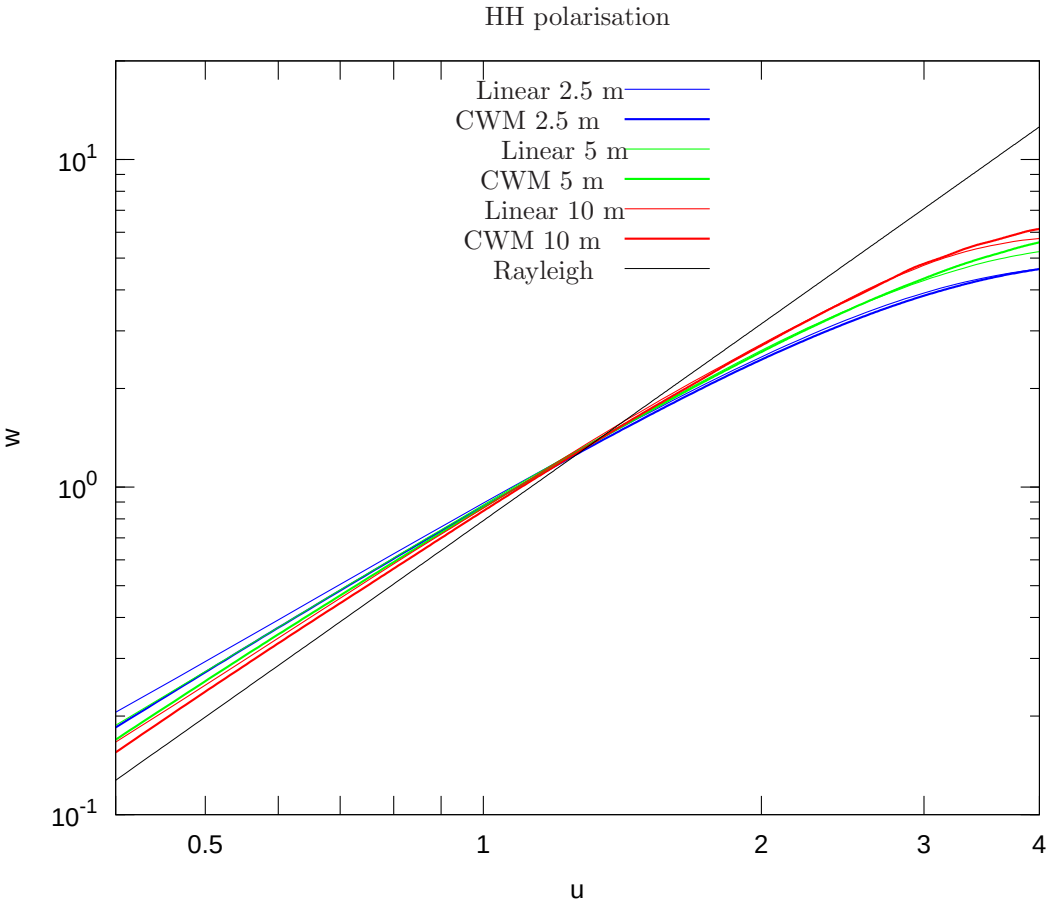

Figure 9: Tail of the cumulative distribution in Weibull paper for different resolution cells.